Applied Catalysis B: Environmental 330 (2023) 122639

Contents lists available at ScienceDirect

Applied Catalysis B: Environmental

journal homepage: www.elsevier.com/locate/apcatb

# Study on hydrolase mechanism of copper compound nanoparticles and its application in the evaluation of gut bacteria in aquatic environment

Zhixuan Yu [a,b], Jinxing Chen [a], Daiyong Chao [a], Xiaoxuan Sun [a,b], Ling Liu [a,*], Shaojun Dong [a,b,**]

[a] State Key Laboratory of Electroanalytical Chemistry, Changchun Institute of Applied Chemistry, Chinese Academy of Sciences, Changchun, Jilin 130022, PR China
[b] University of Science and Technology of China, Hefei, Anhui 230026, PR China

ARTICLE INFO

*Keywords:*
Catalytic mechanism
Hydrolases-like
Biofeedback regulation
Gut bacterial contamination
Aquatic environment

ABSTRACT

Conversing proteinaceous enzyme behavior into nanomaterials is intriguing academically, but the threshold from mimicry to accessing sophisticated biological entities has not yet been crossed. Herein, we disclosed the pan-glycoside hydrolases-like (p-GHs-like) activities of $Cu_3P$ and $Cu_2O$ nanoparticles and decently confirmed their consistent catalytic mechanism as natural glycoside hydrolase, that is, the precise bond breaking, anomeric carbon configuration and catalytic attack mode. We then introduced p-GHs-like NPs into *Escherichia coli* to establish a feedback regulatory model for the β-D-glucuronidase (expressed by uidA) that was initially expressed in trace amounts. An upregulation of uidA from 72 to 1000 counts was induced by the p-GHs-like activities via pre-released β-glucuronides derivatives, further contributing to 1–2 orders enhancement of the enzyme production. We unearthed the specific catalytic mechanism to unlock a black box of enzyme-like inorganic feedback on the natural enzyme synthesis process, pushing mimicry leaped to physiological behavior.

## 1. Introduction

Glycoside hydrolases (GHs) catalyze the hydrolysis of specific glycosidic compounds to the corresponding glycosyl and aglycons, and play a pivotal role in biomedicine (e.g. targets for cancer [1,2] and diabetes [3]) and industry (e.g. biofuel, detergent production and detection), especially in evaluation of environmental fecal microorganism contamination from gut bacteria [4]. For engineering the hydrolysis of glycosides, the strict reaction conditions are required to combat the opportunistic instability of natural enzymes, which greatly increases the difficulty of operation and the cost in industry [5]. For example, some hydrolytic enzymes are naturally expressed with a very low basic level in a medium without inducers, which hinders the applications that require the rapid expression of these enzymes, such as the β-D-glucuronidase (GUS) used for *Escherichia coli* (*E. coli*) detection [6,7]. Another example is β-D-glucosidase (β-GC), a main enzyme in the degradation of cellobiose, which has been demonstrated to be a rate-limiting step in the degradation of cellulose to produce biomass, one of the future alternatives to fossil fuels [8,9]. However, this natural enzyme requires some necessary catalytic physiological conditions and low temperature transport in order to keep an effective work [10]. To address these problems, hydrolase-like inorganic substitutors, mainly nanomaterials called as nanozymes now, provide a promising strategy with higher environmental tolerance and long-term stability than their natural counterparts [11–13].

Obviously, if we find some nanomaterials with the same catalytic mechanism as natural enzymes, we can expect that their pre-reaction in vitro will release special factors, so as to tandem a positive feedback regulation of natural enzymes expression, which can perfectly solve the above problems. However, so far, there are only a few reports on GHs-like nanomaterials [14,15], and much fewer studies on the catalytic mechanism, let alone the access of sophisticated biological entities. Therefore, we intend to drive an opportunity to cross the threshold from mimicry to physiological behavior.

Herein, we summarized the hydrolase-like categories of nanomaterials in recent literature, which mainly included glycosidase [5], lipase [15], amidase/protease [16], nuclease [17], and phosphatase [18]. Then, we found a suitable GHs-like reaction as the research object

* Corresponding author.
** Corresponding author at: State Key Laboratory of Electroanalytical Chemistry, Changchun Institute of Applied Chemistry, Chinese Academy of Sciences, Changchun, Jilin 130022, PR China.
*E-mail addresses:* liuling@ciac.ac.cn (L. Liu), dongsj@ciac.ac.cn (S. Dong).

https://doi.org/10.1016/j.apcatb.2023.122639
Received 4 January 2023; Received in revised form 5 March 2023; Accepted 13 March 2023
Available online 15 March 2023
0926-3373/© 2023 Elsevier B.V. All rights reserved.

to initiate the study, upon identifying $Cu_3P$ and $Cu_2O$ NPs as valid candidates. A pan-glycoside hydrolases-like (p-GHs-like) reaction was established and their catalytic mechanism was studied thoroughly. With the help of their catalytic mechanism consistent with that of natural hydrolase, a feedback regulation model induced by the glycoside derivatives pre-released via the p-GHs-like activities on the expression of relevant original trace mRNA in live bacteria was established.

## 2. Experiment section

### 2.1. Materials and instrumentations

Copper (II) chloride dihydrate ($CuCl_2$•$2H_2O$, 99%), copper (II) nitrate trihydrate ($Cu(NO_3)_2$•$3H_2O$, 99%), sodium selenite ($Na_2SeO_3$, 97%) and thiourea ($(NH_2)_2CS$, 99%) were purchased from Beijing Chemical Works. Copper (Cu, 99.9%) and 4-Nitrophenyl-β-D-glucopyranoside (PNPG, 98%) were purchased from Aladdin. Polyvinylpyrrolidone (PVP, Mw=40000), 3,3′5,5′-tetramethylbenzidine (TMB, 99%) and peroxidase from horseradish (HRP, 300 U/mg) were bought from Sigma-Aldrich. β-D-glucosidase from almonds (20 U/mg) and from *Aspergillus niger* (100 U/g) were purchased from Shanghai yuanye Bio-Technology Co., Ltd. The heavy water ($H_2^{18}O$, 98 atom % $^{18}O$) was purchased from Energy Chemical (Shanghai, China). LIVE/DEAD™ BacLight™ Bacterial Viability Kit (L13152) was purchased from Thermo Fisher. Ultrapure water was used throughout the experiments. LB medium: 10.0 g tryptone, 5.0 g yeast extract and 10.0 g NaCl in 1 L of water, pH 7.0. Minimal medium-MUG (mm-MUG): 5.0 g $(NH_4)_2SO_4$, 0.5 mg $MnSO_4$, 0.5 mg $ZnSO_4$, 100.0 mg $MgSO_4$, 10.0 g NaCl, 50.0 mg $CaCl_2$, 40.0 mg $Na_2SO_3$, 75.0 mg MUG, 5.3 g HEPES-Na and 6.9 g HEPES in 1 L of water, pH 7.2.

Transmission electron microscope (TEM) images were taken on a Hitachi H-8100 EM microscope operated at 100 kV. High-resolution transmission electron microscope (HRTEM) images were obtained using a Talos F200X microscope. Scanning electron microscope (SEM) images were acquired using a Hitachi SU-8020 (Japan) field-emission microscope. XRD analysis was carried out on an X-ray diffractometer (Bruker D8 Advance) with Cu Kα. X-ray photoelectron spectroscopy (XPS) was collected on an ESCALABMKII (VG Co., UK) spectrometer with an Al Kα excitation source. UV–vis absorption spectra were recorded on a Cary 60 UV–vis spectrophotometer (Varian). The fluorescence spectra were determined using a Cary Eclipse fluorescence spectrophotometer (Agilent Technologies) and an enzyme-labeling instrument (Tecan). The permeability of the bacteria was imaged by confocal laser scanning microscopy (CLSM, Nikon, C2, Japan).

### 2.2. Nanomaterials preparation

The $Cu_2O$ NPs were synthesized according to a reported method [19]. In a typical experiment, 50 mL 0.01 M $CuSO_4$•$5\ H_2O$ and 50 mL 0.1 M 2-methylpyridine were added in a 500 mL round bottom flask under constant stirring. After the solution turned deep blue, 50 mL 0.1 M glucose and 100 mL 1 M NaOH were added to the mixture solution (80 °C) for 5 min to synthesize $Cu_2O$ NPs. The CuO NPs were synthesized according to an aqueous-based chemical precipitation method [20]. And the $Cu_3P$ NPs were synthesized according to the method we previously reported [21]. 20 mg CuO NPs and 300 mg $NaH_2PO_2$ were placed at each end of a crucible boat with a cover and then calcined at 300 °C for 2 h with the heating rate of 5 °C/min under $N_2$ atmosphere in a tube furnace. The CuS and $Cu_2S$ NPs were synthesized according to a reported method [22]. 2 mmol $Cu(NO_3)_2$•$3\ H_2O$ was dissolved in 25 mL dimethyl sulfoxide (DMSO), then 0.4 g PVP and 4 mmol thiourea were added, followed by transfer into a 40 mL Teflon-lined stainless steel autoclave. The autoclave was sealed and maintained at 120 °C for 20 h to synthesize CuS NPs. The synthesis procedure of $Cu_2S$ NPs was similar to the CuS NPs, except that N, N-dimethylformamide (DMF) was used instead of DMSO. The CuSe NPs were synthesized according to a reported method [23]. 2 mmol $Na_2SeO_3$ and 4.8 mL hydrazine hydrate were added in 50 mL ultrapure water, and then mixed with the solution prepared by dissolving 1.8 mmol $CuCl_2$•$2\ H_2O$ in 50 mL ultrapure water with magnetic stirring. After 5 min stirring, the mixture solution was placed in a microwave oven heated for 15 min to synthesize CuSe NPs. The $Cu_2Se$ NPs were synthesized according to a reported method [24]. 0.58 mmol $Cu(NO_3)_2$•$3\ H_2O$ and 0.29 mmol $Na_2SeO_3$ were dissolved in 55 mL ultrapure water, then 8 mL hydrazine hydrate was added to the mixture solution under magnetic stirring. After 20 min stirring, the mixture solution was transferred into the Teflon-lined stainless steel autoclave. The autoclave was sealed and maintained at 180 °C for 24 h to synthesize $Cu_2Se$ NPs.

### 2.3. Characterization of p-GHs-like activities

In a typical experiment, for the chromogenic substrate PNPG, 100 μL 100 mM different buffer solutions (acetate buffer, pH = 3–6; Tris-HCl buffer, pH = 7–8; carbonate buffer, pH=9–11), 200 μL $Cu_2O$ NPs (1 mg/mL), 500 μL PNPG (2 mM) and 200 μL ultrapure water were added sequentially into a 1.5 mL tube. After the hydrolysis reaction, an equal volume of carbonate buffer (100 mM, pH 11) was added to terminate the hydrolysis reaction and then passed through a 0.22 μm filter membrane to remove particles. The catalytic hydrolysis of PNPG was studied by monitoring the absorbance at 400 nm. And for the fluorogenic substrate MUG, the final concentration of MUG was 0.2 mM. The excitation wavelengths of MUG and 4-MU were 320 and 366 nm, respectively.

### 2.4. Catalytic mechanism of p-GHs-like NPs

To detect •OH radicals, 100 μL coumarin (10 mM), 100 μL acetate buffer solution (100 mM, pH 4.0), 200 μL $Cu_2O$ NPs (1 mg/mL) and 600 μL ultrapure water were added sequentially into a 1.5 mL tube. After the reaction, the fluorescence emission spectrum was measured after mixing 200 μL reaction solution with 800 μL of carbonate buffer (100 mM, pH 11). The excitation and emission wavelengths of 7-hydroxycoumarin were 332 and 460 nm, respectively. To detect $H_2O_2$, 2 mL $Cu_2O$ NPs (1 mg/mL), 1 mL acetate buffer solution (100 mM, pH 4.0), and 8 mL ultrapure water were added sequentially into a 15 mL tube. The mixture solutions were allowed to stand at room temperature for 10 min and then passed through a 0.22 μm filter membrane to remove particles. 20 μL TMB (20 mM) and 20 μL HRP (0.05 mg/L) were added in 1 mL filtrate to determine the $H_2O_2$ generation. The absorption at 650 nm was measured. In a typical experiment, 200 μL $Cu_2O$ NPs (1 mg/mL), 100 μL PNPG (10 mM), 100 μL acetate buffer solution (100 mM, pH 4.0), and 600 μL ultrapure water were added sequentially into a 1.5 mL tube. After the hydrolysis reaction, the mixture solutions were passed through a 0.22 μm filter membrane to remove particles. 100 μL the filtrates were precisely taken out and then removed the solvents completely using a Nitrogen Blowing Concentrator. 100 μL pyridine (anhydrous) was added to solubilize the hydrolyzation products and derivatized with 50 μL BSTFA (containing 1% TMCS) at 100 °C for 1 h and then analyzed by gas chromatography-mass spectrometry (GC-MS). The GC-MS analysis for hydrolysate derivatives was performed using an Agilent 7000D gas chromatograph equipped with an Agilent 5975 mass selective detector (MSD) with an Agilent HP-5 ms capillary chromatographic column (30 m, 250 μm, 0.25 μm). The GC oven temperature was initially 80 °C for 3.0 min, rising to 280 °C at 10 °C/min with a middle hold at this temperature for 5 min, and then rising to 300 °C at 20 °C/min with a final hold at this temperature for 6 min. The helium carrier gas flow rate was 1 mL/min. GC-MS interface temperature was 280 °C and (electron impact) ion source temperature was 230 °C, with 70 eV ionization voltage. For the GC-MS-heavy Water ($H_2^{18}O$) Experiments, the solvent was $H_2^{18}O$.

### 2.5. Feedback regulation model of E. coli

In a typical experiment, the *E. coli* ATCC 25922 was inoculated in the culture medium (75.0 mg of MUG, 10.0 g of tryptone, 8.5 mg of $KH_2PO_4$, 21.8 mg of $K_2HPO_4$, 33.4 mg of $Na_2HPO_4$•7 $H_2O$, 1.7 mg of $NH_4Cl$, 22.5 mg of $MgSO_4$•7 $H_2O$, 0.25 mg of $FeCl_3$•6 $H_2O$, 27.6 mg $CaCl_2$ in 1 L of ultrapure water), once the optimal $Cu_3P$ NPs concentration was determined, added them to the culture medium, and next put them in an incubator at 37 °C for static culture. After incubation, the fluorescence of 4-MU was determined after mixing the bacterial liquid and carbonate buffer (100 mM, pH 11) at the ratio of 1:1 to indirectly calibrate the initial concentration of *E. coli*. After incubation of bacteria ($OD_{600} = 0.5$) and different materials (100 μg/mL) for an hour at 37 °C. The *E. coli* ATCC 25922 was collected and stained with SYTO 9 and propidium iodide (PI) for 15 min in the dark and visualized by a confocal fluorescence microscopy.

### 2.6. Gene analysis and mRNA expression

NPs with certain concentrations were added into the mm-MUG medium, then, *E. coli* was inoculated with the final $OD_{600} = 0.08$ (37 °C). After incubations for 3 h, *E. coli* was collected by centrifugation and the real-time nodes of gene expression were fixed by freezing the centrifugal sediments in liquid nitrogen and transporting by dry ice protection. Transcriptome analysis was carried out by high-throughput sequencing (HTS) technique on a NovaSeq platform (Illumina, USA). FastQC and Trimmomatic were used for quality control. Bowtie2 was used to compare clean reads of each sample with non-redundant gene sets. RSeQC was used to analyze the replicate-sequences, then Qualimap and BED Tools were used for statistical analysis of gene coverage and genome sequencing. BSFtools and Rockhopper were used for gene structure analysis. FeatureCounts was used for assessing the gene expression by referring the known genetic model >NC 000913.3: c366305–363231. The genes were annotated by using the NCBI (NR, NT and COG), CAZy, GO, KEGG, Uniprot, Ensemble, Biomart, PFAM and CDD database. All results were shown in the legend and their p-values were enclosed. Gene sequence data with log2(Fold Changes) and p-values were identified by R package DEGseq 1.26.0. TPM statistic was calculated by using featureCounts 1.6.0. All heatmaps were composed using of OmicStudio online tools and the related statistics were accorded to the gene analysis.

### 2.7. DFT calculations

DFT calculations and their statistical analysis were carried out using of Material Studio 2020 with Dmol3 module. A surface model was cleaved from this supercell to simulate the (111) surface of the structure of CuO and $Cu_2O$ NPs. The generalized gradient approximation method with Perdew-Burke-Ernzerhof function was employed to describe the interactions between core and electrons. In the vertical direction, a vacuum layer of about 10 Å in thickness was introduced for the surface. The force and energy convergence criterion were set to 0.002 Ha/Å and $10^{-5}$ Ha, respectively. When the optimization was completed, the transition states were located utilizing the well-known linear synchronous transit (LST) and quadratic synchronous transit (QST) methods. After the LST/QST calculations, the frequency calculations were performed. A true transition state from LST/QST calculations was confirmed by a single negative frequency. The free energy corrections were accomplished with dmol3 at a temperature of 298.15 K.

## 3. Results and discussion

### 3.1. Hydrolytic reactions catalyzed by p-GHs-like NPs

Herein, through the literature data-informed analysis [14,25,26], we synthesized a series of copper compound nanoparticles ($Cu_nX$ NPs, X = P, O, S, Se, Fig. S1 to S7) and screened their glycosidic bonds-catalyzed activities by employing p-nitrophenyl-β-D-glucopyranoside (PNPG) and 4-methyl-umbelliferyl-β-D-glucuronide (MUG) as the reaction substrates (Fig. 1a-e). The PNPG and MUG are artificial conjugates, which are specially hydrolyzed by natural β-GC and GUS to release chromogenic label 4-nitrophenol (4-NP) and fluorogenic label 4-methylumbelliferone (4-MU), respectively. The UV–vis spectra of PNPG showed a constant peak at 300 nm (Fig. S8a), while the absorption peak values of 4-NP varied with pH and no longer changed when pH> 9 (Fig. S8b), which was used for judging the 4-NP in a solution. As shown in Fig. 1b, after adding $Cu_2O$ NPs (or $Cu_3P$ NPs) to the PNPG solution, a new peak at 400 nm appeared, indicating 4-NP was produced. In the GC-MS, the peaks at 12.24 min, 13.81 min, 14.56 min, and 22.35 min were assigned to 4-NP, α-D-glucose, β-D-glucose, and PNPG, respectively (Fig. 1c), more directly indicating that PNPG was cloven by the $Cu_2O$ NPs. In the fluorescence spectra, the excitation/emission for MUG and 4-MU were 320 nm/376 nm (ex/em) and 366 nm/450 nm (ex/em), respectively (Fig. S9). In the presence of $Cu_2O$ NPs (or $Cu_3P$ NPs), the emission peak at 450 nm was increased significantly, indicating that the 4-MU was produced (Fig. 1d). In the GC-MS spectra, the peak at 15.81 min and 26.71 min were assigned to the 4-MU and MUG, respectively, where 16.01 min and 16.51 min correspond to D-glucuronic acid (GA) (Fig. 1e). The present results indicated that $Cu_2O$ and $Cu_3P$ NPs showed the activity for cleaving the glycosidic bonds and an appropriate substrate as label molecule can be selected according to different characterization requirements in the subsequent experiments.

We then determined the possible reaction types of the glycosidic bond cleavage by the present NPs. $Cu_2O$ NPs were already demonstrated to possess the activity for generating OH radical (•OH, in Fig. S10a, b) that could cut glycosidic bonds through their oxidative activity [27]. Herein, isopropanol alcohol (IPA) was therefore employed to trap •OH to test whether it acted as a glycosidic bond cutter, and which it did not (Fig. S10c). Similarly, $H_2O_2$ and $O_2$ were also demonstrated to have no effect (Fig. S10c, d). Considering that the slow disproportionation reaction of $Cu_2O$ NPs can generate Cu and CuO under acidic conditions, they were also added to the PNPG solution and no catalytic activity was obtained (Fig. S11). Besides, the $Cu^{2+}$ effect in the present system was also excluded (Fig. S12).

After excluding the above possible reaction types, we adopted heavy oxygen water ($H_2^{18}O$) instead of ordinary water ($H_2^{16}O$) to analyze the cleaving sites of PNPG and to trace whether $H_2O$ was involved in the new bonds. The mass spectrogram of the 4-NP trimethylsilyl derivative produced in this reaction was completely consistent with that of the standard (Fig. S13a), indicating that O atom was not in newly formed 4-NP. The peak $m/z = 193$ in the mass spectrogram showed that $^{18}O$ appeared in the D-glucose derivative fragments (Fig. 1 f, g, full spectra in Fig. S13b, c), that was, in this $Cu_2O$ NPs catalyzed reaction, a molecule of $H_2^{18}O$ was cloven and the hydroxyl (-$^{18}$OH) was added to the side of the D-glucose. Thus, the reaction type was determined to be hydrolysis, and the acetal (or ketal) bond near the glycosidic end was confirmed as the exact breaking bond, which was consistent with that of the hydrolysis catalyzed by native β-GC. There was an explanation for the peak $m/z = 191$ (in Fig. 1 f, g) assigned to the $^{16}O$-glucose derivative fragments, which mainly came from the raw $^{16}O$-glucose (about 1.21%) in PNPG and the 2% $H_2^{16}O$ in heavy oxygen water (98% purity). The preferential catalysis of $H_2^{16}O$ (Table S1) by both $Cu_2O$ NPs and β-GC was attributed to its low activation energy. Furthermore, the configuration of anomeric carbon of the produced glucose showed inversion and retention forms in the reactions catalyzed by both $Cu_2O$ NPs or β-GC, (Fig. 1 h, i). The above results indicated that PNPG underwent similar reactions catalyzed by p-GHs-like NPs and natural β-GC, specifically, the consistent cleaving site of the acetal (or ketal) bond and the same anomeric carbon configuration changes.

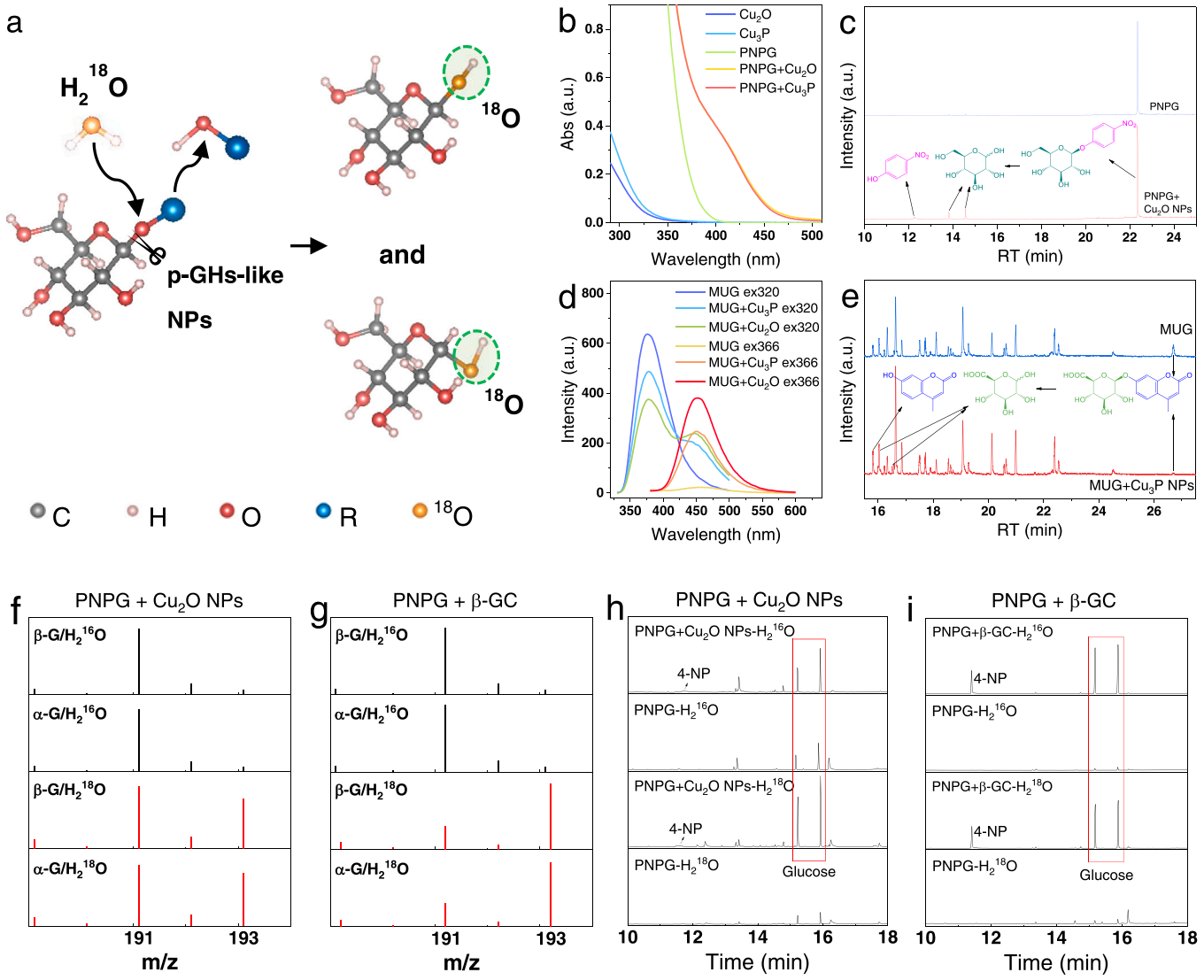


**Fig. 1.** Glycosidic bonds hydrolyzed by p-GHs-like NPs. (a) Schematic illustration of the proposed reaction sites and configurations of glycosidic bonds cloven by the p-GHs-like NPs. (b) UV–vis absorption spectra of PNPG treated with $Cu_2O$ NPs or $Cu_3P$ NPs, and (c) their representative GC-MS spectra. (d) Fluorescence spectra of MUG treated with $Cu_2O$ NPs or $Cu_3P$ NPs, and (e) their representative GC-MS spectra. Mass spectrometry of glucose produced from PNPG catalyzed by (f) $Cu_2O$ NPs catalysis and (g) β-GC, α- and β-G are short for α- and β-glucoses, respectively. Representative GC-MS spectra for PNPG catalyzed by (h) $Cu_2O$ NPs and (i) β-GC. All experiments were repeated 3 times independently with similar results.

### *3.2. Catalytic mechanism of p-GHs-like NPs*

Following the above studies, we exactly confirmed the two atoms (C-O near the glycosidic end), where the glycosidic bond has been broken and allowed the aglycons to leave. In addition, for the natural GHs, two core residues were in charge of the catalytic reaction (Fig. 2a). One of them acted as the nucleophile to attack the carbon center of the glycosidic bond, and the other attacked the leaving glycosidic oxygen just like a general base [28]. Referring to this catalytic mechanism, and further considering the electronegativity of the two atoms at the cloven sites (C-O), the oxygen atoms of the NPs can be presupposed to act as a nucleophile to attack the carbon atoms of the glycosidic bond, while the copper atom or the adsorbed proton on the NPs surface should have the affinity with the glycosidic oxygen. Therefore, two theoretically feasible attack paths for the reaction of PNPG catalyzed by p-GHs-like NPs were drawn out (Fig. 2b).

We then conducted density functional theory (DFT) calculations to extrapolate the attacking paths. CuO NPs were used as a comparative study due to their structural similarity with $Cu_2O$ NPs and the strongest crystal plane (111) in the XRD pattern was used for the DFT calculations. For the two types of NPs, path II was an exothermic process for both α and β conformational products, which was unfavorable to the catalyzed reaction (Fig. 2c, d). By contrast, path I was thermodynamically preferred in the hydrolysis of PNPG catalyzed by these NPs. Besides, for producing α and β conformational products, the total energy barriers of 89.3 and 89.3 kcal/mol, and 19.5 and 17.0 kcal/mol were required by the CuO and $Cu_2O$ NPs, respectively (Fig. 2c, d, more intermediate structures, and their single point energy and free energy were listed in the Tables S2 and S3). These energy barriers showed that $Cu_2O$ NPs had a lower energy barrier than CuO NPs, which were consistent with the experimental results of the spectra measurement. Thus, the $Cu_2O$-path I showed the advantage in comparison. The free energies in this pathway were similar for the two conformational products and just with slightly different due to the inversion of the configuration at IM-1α, indicating the same opportunity for both α and β products, which was also consistent with the GC-MS results. Thus, the catalytic mode driven by a combined nucleophilic and electrophilic attack was confirmed by the DFT calculation that was all matched with the experimental results.

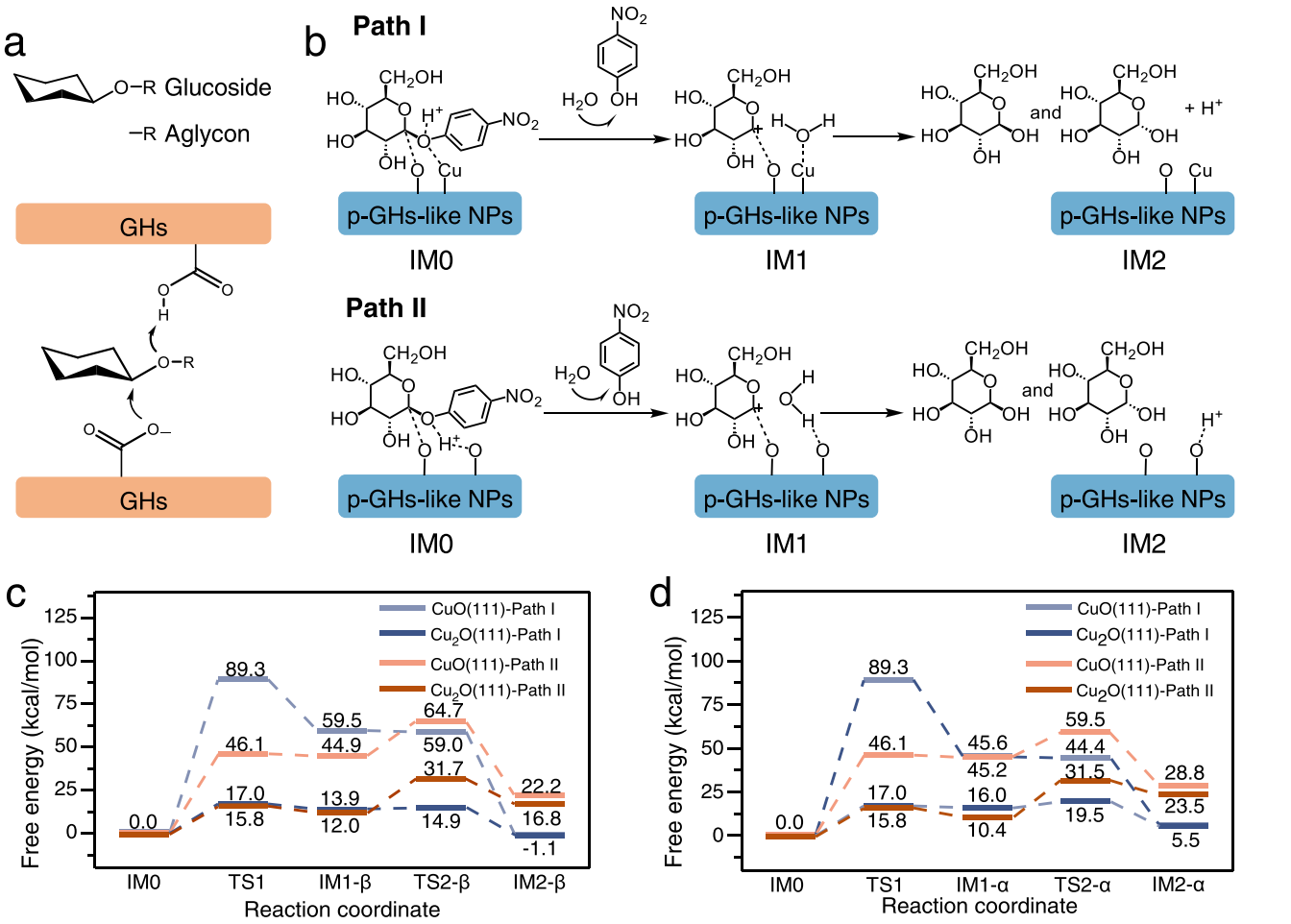


**Fig. 2.** Catalytic mechanism of p-GHs-like NPs. (a) General catalytic mechanisms for typical GHs. (b) Two possible attacking paths of the PNPG hydrolysis catalyzed by $Cu_2O$ and CuO NPs, and the corresponding energy profiles for the (c) β and (d) α conformation of the produced glucose.

### 3.3. *Do p-GHs-like NPs behave like a proteinaceous enzyme?*

We further studied the catalytic performances of the p-GHs-like NPs and determined whether they behaved like a proteinaceous enzyme. Firstly, the specificity and selectivity of the present p-GHs-like NPs were studied. Among a series of $Cu_nX$ NPs, $Cu_3P$ and $Cu_2O$ NPs were identified to validly hydrolyze PNPG (Fig. 3a and Fig. S14), noting that they were more similar in structure than the other materials (structures of the seven $Cu_nX$ NPs in Fig. S1 to S7), while the other prepared NPs showed no GHs-like activities. Substrate selectivity was investigated by catalyzing a variety of compounds containing 4-NP probes, and experimental data showed that the present NPs tended to hydrolyze glycosidic bonds (Fig. 3b, detail in Table S4), which was why we defined the present materials as p-GHs-like NPs. And we presumed that the different crystal structures, including crystal plane, bond angle and bond length, possessed different absorbability with substrates and caused for different energy barriers for new bond formation, and coupling a certain selectivity toward substrate molecules [29]. The other remarkable property of natural enzymes was their reusability, and herein, $Cu_2O$ NPs were found to keep their catalytic activities 90–100% in six catalytic cycles (Fig. 3c). Interestingly, the catalytic activity was slightly enhanced after the first cycle and that was because of the $Cu_2O$ NPs surface became rough due to the etching of acetate buffer solution, although they largely maintained their morphology after six cycles (insert of Fig. 3d), especially the XRD results showed that the compositions and crystal structures of the NPs were completely kept. The results indicated that $Cu_2O$ NPs could be reused with good stability.

We had also studied the reaction kinetics of the p-GHs-like NPs. The hydrolase-like activity of $Cu_2O$ NPs was increased with the temperature from 30 to 90 °C (Fig. 3e) in the optimized acidic conditions (Fig. 3f). The substrate conversion was a continuous process affording a buildup of the product, but with a gradually decreased catalytic rate over time (Fig. 3g). The reaction rate was significantly improved by increasing the concentration of both catalyst and substrate (Fig. S15). But the NPs showed no obvious hydrolase-like activity in those commonly used organic solvents (Fig. S16). According to the Michaelis–Menten curve, the enzyme kinetic constants $K_m$ (Michaelis constant) and $V_m$ (maximal velocity) were calculated as 1.69 mM and 10.76 μM/min for $Cu_2O$ NPs (Fig. 3h and Fig. S17), 0.45 mM and 22.01 μM/min for the β-GC from *Aspergillus niger* (*A. niger*) source (Fig. S18), and 3.13 mM and 47.90 μM/min for the β-GC from almonds source (Fig. S19), respectively. $Cu_3P$ NPs also showed similar reaction kinetics with that of $Cu_2O$ NPs (Fig. S20). It should be taken into account of the catalytic rates and the turnover number (or TON), the Michaelis–Menten curve was thereby only used as a reference to reflect the kinetic characteristics for the p-GHs-like NPs. Furthermore, the present $Cu_2O$ NPs successfully hydrolyzed cellobiose, maltose, sucrose, and lactose (Fig. 3i), but not polysaccharides (Fig. S21). Combined with these results, the present p-GHs-like NPs are comparable to their natural enzymes in terms of the catalytic capacity and can catalyze natural disaccharides.

### 3.4. *Do p-GHs-like NPs participate in physiological activities?*

From the above results, we determined that the present p-GHs-like NPs definitely possess the properties of natural GHs. However, they were not born through a genetically coded process, so this raised a question of

a

| Hydrolysis of PNPG | |
|---|---|
| $Cu_3P$ NPs | Yes |
| $Cu_2O$ NPs | Yes |
| CuO NPs | No |
| $Cu_2S$ NPs | No |
| CuS NPs | No |
| $Cu_2Se$ NPs | No |
| CuSe NPs | No |
| Cu NPs | No |

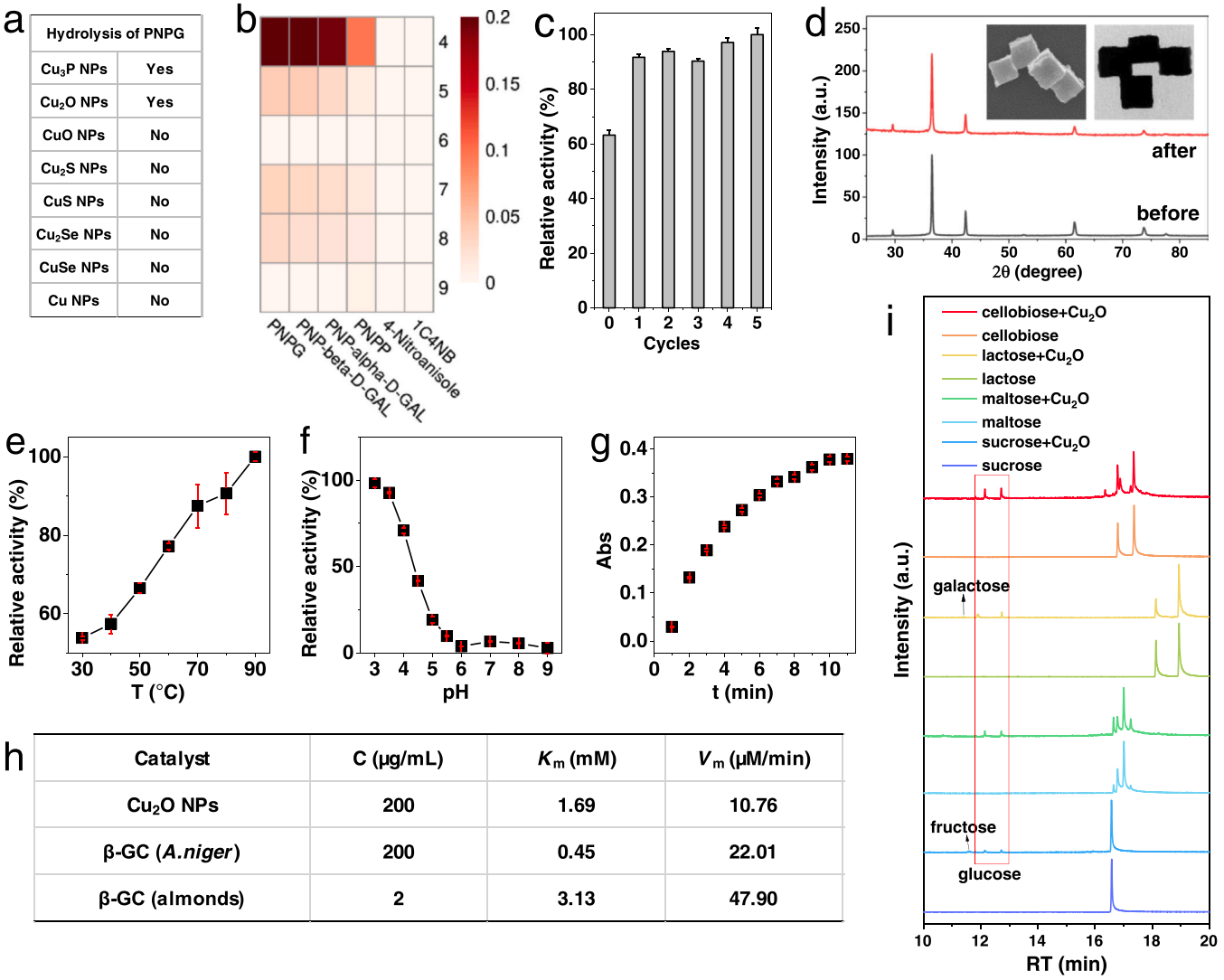


h

| Catalyst | C (μg/mL) | $K_m$ (mM) | $V_m$ (μM/min) |
|---|---|---|---|
| $Cu_2O$ NPs | 200 | 1.69 | 10.76 |
| β-GC (*A.niger*) | 200 | 0.45 | 22.01 |
| β-GC (almonds) | 2 | 3.13 | 47.90 |

**Fig. 3.** Performances of p-GHs-like NPs. (a) Determining different $Cu_nX$ NPs for hydrolyzing PNPG, Cu NPs are nanopowders. (b) Different catalytic substrates that containing 4-NP probe, pH 4–9. (c) The activities of $Cu_2O$ NPs to hydrolyze PNPG in 6 recycles, and the (d) XRD patterns of the NPs before (black line) and after (red line) reactions, insert, the SEM and TEM images of $Cu_2O$ NPs after reactions. The catalytic properties under different (e) temperatures, (f) pH, and (g) time. (h) Steady-state kinetic parameters of $Cu_2O$ NPs and the natural β-GC from almonds and *A. niger*. (i) The representative GC-MS spectra for typical disaccharides catalyzed by $Cu_2O$ NPs. The error bar represents the standard deviation of 5 independent measurements.

whether p-GHs-like NPs could participate in life activities and act the feedback regulation on the expression of their natural GHs. Herein, a study model was established by employing MUG as the substrate molecular, which was catalyzed by $Cu_3P$ NPs to release 4-MU as the signal to indicate the GUS expression in *E. coli*, while the corresponding transcriptomic information was synchronously analyzed by high-throughput sequencing (HTS). Under the optimized conditions (Fig. S22), the net fluorescent intensity of 4-MU obtained by adding $Cu_3P$ NPs was higher than that of the control with 1–2 orders (Fig. 4a), indicating that more MUG molecules were hydrolyzed. Meanwhile, the *E. coli* concentrations were same after treating by different concentrations of $Cu_3P$ NPs (Fig. 4b), indicating no proliferation or sacrifice of the bacteria in this reaction system. Therefore, the increase of the fluorescent signals was most likely to depend on the upregulated expression of the related enzymes, which is GUS decided by the glucuronic acid side of MUG. To verify, the HTS further used to analyze the related gene expressions, after the addition of $Cu_3P$ NPs, the uidA, uidB, and uidC for encoding and transporting GUS were increased from 72 to 1000 counts, 34 to 493 counts, and 12 to 259 counts, respectively (Fig. 4c, Table S5), and with a strong TPM statistical significance (Fig. 4d). Thus, we confirmed that there was a positive feedback regulation on uidX (X = A, B and C) gene transcription, as well as the GUS expression, by the p-GHs-like NPs.

Then, we illustrated the feedback regulatory model of GUS expression in Fig. 4e. In path (1), the initial one for this strain in the natural condition, *E. coli* was difficult to produce GUS. In path (2), with the p-GHs-like activities of NPs, the MUG and other ingredients in the medium solution were hydrolyzed to produce GA and its derivatives. The GA (Fig. S23) and β-glucuronides [30,31] were demonstrated to have the abilities to induce GUS expression in *E. coli*, and here, they were collectively termed GA-like derivatives. On the other side, the present $Cu_3P$ NPs had already been demonstrated to have lipid peroxidation (LPO) activities [21], which coupled with the p-GHs-like activities, thus enhancing the permeability of *E. coli* membrane (Fig. S24), leading to a higher mass transfer to give a further help for the detected signals. Besides, the other $Cu_nX$ NPs without p-GHs-like activities did not show an advanced effect on the uidX gene expression (total genes were provided in Appendix B). Then, the p-GHs-like properties of $Cu_3P$ NPs were adopted to help the *E. coli* detection in the traditional enzyme method and the results were satisfied (Fig. S25). The present result showed a model for nanomaterials to play the feedback regulation on gene

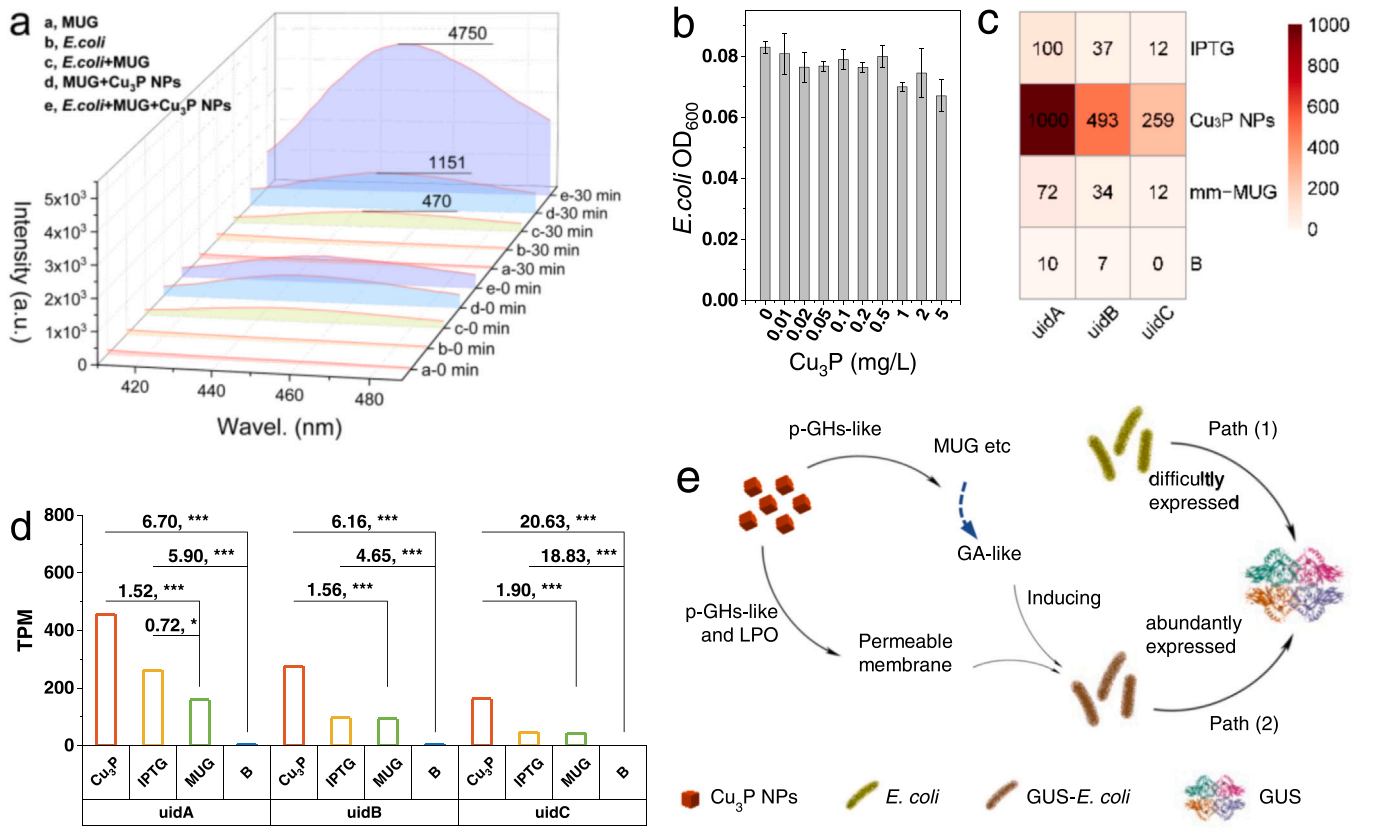


**Fig. 4.** Feedback regulatory model for GUS expression in living bacteria. (a) 4-MU fluorescence intensities in the *E. coli* solutions, and (b) *E. coli* density treated with different concentrations of $Cu_3P$ NPs. 37 °C, 75 mg/L MUG for all tests. The error bars represent the standard deviation of 6 independent measurements. (c) Hotmap of the counts of uidA, uidB and uidC. B, in LB medium; mm-MUG, minimal medium-MUG; and the other test materials were added into the mm-MUG. (d) TPM changes of uidA, uidB and uidC interfered with different materials. The numbers on the straight lines are log2(Fold Changes); * ** : $p < 0.0001$; * : $p = 0.015$; TPM: Transcripts Per Million. (e) Schematic illustration of the feedback regulatory model for GUS expression in living bacteria.

expression and provided an opportunity to cross a threshold from mimicry to physiological behavior.

## 4. Conclusions

With the development of nanozymes, their definitions and uses have become clear and improved [10,32]. The research on new nano-hydrolase-like type is in the foreground, which is bound to be the next focus of attention [33,34]. However, in-depth research on the mechanism, especially on the bond breaking and conformation is still lacking. For establishing a method to explore the catalytic mechanism of the nanomaterials, we chose the hydrolytic enzyme type due to it can be easily studied by the label of heavy oxygen water, and used a large number of traditional means that for natural enzyme studies, and conducted the DFT calculations based on the hydrolyzed sites determined by the isotope-label method. These research methods can give accurate measurement results and the relevant literatures have strongly referred and discussed values [35–38]. As can be seen from the results, the deep science information was given, including the specific reactions of the substrate molecules, and how NPs played as the natural enzymes function [32,39].

Another advance of our work is coupling the chemical reactions with synchronical gene transcript, to explore the contribution of enzyme-like functions of nanomaterials to biofeedback regulation. To interpret the gene analysis methods here, the gene sequences obtained by the referred analysis were different with those by the De novo (a typical lacZ sequences for comparing analysis methods were provided in Appendix C), but this did not affect the determination of the final results. It should be known that, beyond uidX genes, a batch of other gene expressions were also changed with the present NPs intervention (Fig. S26). Herein, we admit the limitations of this work, although the overall data indicated that the imitation by inorganic substitutes achieved an exactly consistent mechanism with natural enzyme, the physiological activities such as selectivity and feedback regulation were only marginally approximate. A main reason is that the feedback pathway of enzyme-like nanomaterials is still in a black box, although we have made certain explorations, more intermediate substances or related matters are waiting for exploring.

## CRediT authorship contribution statement

Z.Y. and L.L. initiated and designed the research. Z.Y. and J.C. performed the experiments and analyzed the data. Z.Y., J.C. and D.C. contributed materials and analysis tools. Z.Y. and X.S. wrote the manuscript. L.L. and S.D. established the final version of the paper. S.D. supervised the project. All authors contributed to the writing of the manuscript, discussion of the results and implications, and editing of the manuscript at all stages. All authors have given approval to the final version of the manuscript.

## Declaration of Competing Interest

The authors declare that they have no known competing financial interests or personal relationships that could have appeared to influence the work reported in this paper.

## Data Availability

Data will be made available on request.

## Acknowledgements

This work was financially supported by the National Natural Science Foundation of China (Nos. 22274146, 22206182, U21A2037, and 22074137), Department of Science and Technology of Jilin Province (Nos. 20220508098RC and 2021SYHZ0036). We thank Baofeng Liu and Wenbing Xie (National Analytical Research Center of Electrochemistry and Spectroscopy, CIAC, CAS) for fruitful discussions about GC-MS and gas chromatography, and Tianle Zheng and the High Performance Computing Center of Shanghai University and the Shanghai Engineering Research Center of Intelligent Computing System (No.19DZ2252600) for providing computing resources, technical support and discussions, and NGS Department of Sangon Biotech (Shanghai) Co., Ltd for their technical support and discussions of gene analysis..

## Appendix A. Supporting information

Supplementary data associated with this article can be found in the online version at doi:10.1016/j.apcatb.2023.122639.

## References

[1] Q. Liu, J. Li, W. Zhang, C. Xiao, S. Zhang, C. Nian, J. Li, D. Su, L. Chen, Q. Zhao, H. Shao, H. Zhao, Q. Chen, Y. Li, J. Geng, L. Hong, S. Lin, Q. Wu, X. Deng, R. Ke, J. Ding, R.L. Johnson, X. Liu, L. Chen, D. Zhou, Glycogen accumulation and phase separation drives liver tumor initiation, Cell 184 (2021) 5559–5576.

[2] C.F. Labuschagne, R. Smith, N. Kumar, M. Allsworth, B. Boyle, S. Janes, P. Crosbie, R. Rintoul, Breath biopsy early detection of lung cancer using an EVOC probe targeting tumor-specific extracellular $\beta$-glucuronidase, J. Clin. Oncol. 40 (2022).

[3] J. Balaich, M. Estrella, G. Wu, P.D. Jeffrey, A. Biswas, L. Zhao, A. Korennykh, M. S. Donia, The human microbiome encodes resistance to the antidiabetic drug acarbose, Nature 600 (2021) 110–115.

[4] J. Zhao, Y. Xu, W. Wang, J. Griffin, K. Roozeboom, D. Wang, Bioconversion of industrial hemp biomass for bioethanol production: a review, Fuel 281 (2020), 118725.

[5] R. Walther, A.K. Winther, A.S. Fruergaard, W. van den Akker, L. Sorensen, S. M. Nielsen, M.T. Jarlstad Olesen, Y. Dai, H.S. Jeppesen, P. Lamagni, A. Savateev, S. L. Pedersen, C.K. Frich, C. Vigier-Carriere, N. Lock, M. Singh, V. Bansal, R.L. Meyer, A.N. Zelikin, Identification and directed development of non-organic catalysts with apparent pan-enzymatic mimicry into nanozymes for efficient prodrug conversion, Angew. Chem. Int. Ed. 58 (2019) 278–282.

[6] J.B. Burnet, Q.T. Dinh, S. Imbeault, P. Servais, S. Dorner, M. Prevost, Autonomous online measurement of β-D-glucuronidase activity in surface water: is it suitable for rapid *E. coli* monitoring? Water Res 152 (2019) 241–250.

[7] R.D.G. Ferreira, A.R. Azzoni, S. Freitas, Techno-economic analysis of the industrial production of a low-cost enzyme using *E. coli*: the case of recombinant β-glucosidase, Biotechnol. Biofuels 11 (2018) 81.

[8] L. Chen, Y. Liao, Z. Guo, Y. Cao, X. Ma, Products distribution and generation pathway of cellulose pyrolysis, J. Clean. Prod. 232 (2019) 1309–1320.

[9] N. Rodriguez Quiroz, A.M.D. Padmanathan, S.H. Mushrif, D.G. Vlachos, Understanding acidity of molten salt hydrate media for cellulose hydrolysis by combining kinetic studies, electrolyte solution modeling, molecular dynamics simulations, and $^{13}$C NMR experiments, ACS Catal. 9 (2019) 10551–10561.

[10] Y. Wu, W. Xu, L. Jiao, W. Gu, D. Du, L. Hu, Y. Lin, C. Zhu, Nanobiocatalysis: a materials science road to biocatalysis, Chem. Soc. Rev. 51 (2022) 6948–6964.

[11] L. Gao, J. Zhuang, L. Nie, J. Zhang, Y. Zhang, N. Gu, T. Wang, J. Feng, D. Yang, S. Perrett, X. Yan, Intrinsic peroxidase-like activity of ferromagnetic nanoparticles, Nat. Nanotechnol. 2 (2007) 577–583.

[12] B. Xu, H. Wang, W. Wang, L. Gao, S. Li, X. Pan, H. Wang, H. Yang, X. Meng, Q. Wu, L. Zheng, S. Chen, X. Shi, K. Fan, X. Yan, H. Liu, A single-atom nanozyme for wound disinfection applications, Angew. Chem. Int. Ed. 58 (2019) 4911–4916.

[13] Y. Huang, J. Ren, X. Qu, Nanozymes: classification, catalytic mechanisms, activity regulation, and applications, Chem. Rev. 119 (2019) 4357–4412.

[14] S. Li, Z. Zhou, Z. Tie, B. Wang, M. Ye, L. Du, R. Cui, W. Liu, C. Wan, Q. Liu, S. Zhao, Q. Wang, Y. Zhang, S. Zhang, H. Zhang, Y. Du, H. Wei, Data-informed discovery of hydrolytic nanozymes, Nat. Commun. 13 (2022) 827.

[15] P. Nandhakumar, G. Kim, S. Park, S. Kim, S. Kim, J.K. Park, N.S. Lee, Y.H. Yoon, H. Yang, Metal nanozyme with ester hydrolysis activity in the presence of ammonia-borane and its use in a sensitive immunosensor, Angew. Chem. Int. Ed. 59 (2020) 22419–22422.

[16] J. Moons, F. de Azambuja, J. Mihailovic, K. Kozma, K. Smiljanic, M. Amiri, T. Cirkovic Velickovic, M. Nyman, T.N. Parac-Vogt, Discrete $Hf_{18}$ metal-oxo cluster as a heterogeneous nanozyme for site-specific proteolysis, Angew. Chem. Int. Ed. 59 (2020) 9094–9101.

[17] G. Fang, R. Kang, Y. Chong, L. Wang, C. Wu, C. Ge, MOF-based DNA hydrolases optimized by atom engineering for the removal of antibiotic-resistant genes from aquatic environment, Appl. Catal. B: Environ. 320 (2023), 121931.

[18] J.E. Mondloch, M.J. Katz, W.C. Isley 3rd, P. Ghosh, P. Liao, W. Bury, G.W. Wagner, M.G. Hall, J.B. DeCoste, G.W. Peterson, R.Q. Snurr, C.J. Cramer, J.T. Hupp, O. K. Farha, Destruction of chemical warfare agents using metal-organic frameworks, Nat. Mater. 14 (2015) 512–516.

[19] J. Pal, C. Mondal, A.K. Sasmal, M. Ganguly, Y. Negishi, T. Pal, Account of nitroarene reduction with size- and facet-controlled CuO-$MnO_2$ nanocomposites, ACS Appl. Mater. Interfaces 6 (2014) 9173–9184.

[20] S. Konar, H. Kalita, N. Puvvada, S. Tantubay, M.K. Mahto, S. Biswas, A. Pathak, Shape-dependent catalytic activity of CuO nanostructures, J. Catal. 336 (2016) 11–22.

[21] D. Chao, Q. Dong, J. Chen, Z. Yu, W. Wu, Y. Fang, L. Liu, S. Dong, Highly efficient disinfection based on multiple enzyme-like activities of $Cu_3P$ nanoparticles: a catalytic approach to impede antibiotic resistance, Appl. Catal. B Environ. 304 (2022), 121017.

[22] J. Liu, D. Xue, Thermal oxidation strategy towards porous metal oxide hollow architectures, Adv. Mater. 20 (2008) 2622–2627.

[23] I.G. Shitu, J.Y.C. Liew, Z.A. Talib, H. Baqiah, M.M. Awang Kechik, M. Ahmad Kamarudin, N.H. Osman, Y.J. Low, I.I. Lakin, Influence of irradiation time on the structural and optical characteristics of CuSe nanoparticles synthesized via microwave-assisted technique, ACS Omega 6 (2021) 10698–10708.

[24] Y. Zhu, H. Tang, X. Yun, L. Xi, Z. Hu, One-pot hydrothermal synthesis of 3D $Cu_2Se$/CoSe composite as a novel battery-type cathode material with enhanced capacitive properties, J. Alloy. Compd. 866 (2021), 158972.

[25] F. Sabbadin, S. Urresti, B. Henrissat, A.O. Avrova, L.R.J. Welsh, P.J. Lindley, M. Csukai, J.N. Squires, P.H. Walton, G.J. Davies, N.C. Bruce, S.C. Whisson, S. J. McQueen-Mason, Secreted pectin monooxygenases drive plant infection by pathogenic oomycetes, Science 373 (2021) 774–779.

[26] C. Muller, L. Zhang, S. Zipfel, A. Topitsch, M. Lutz, J. Eckert, B. Prasser, M. Chami, W. Lu, J. Du, O. Einsle, Molecular interplay of an assembly machinery for nitrous oxide reductase, Nature 608 (2022) 626–631.

[27] J.A. Hangasky, T.C. Detomasi, M.A. Marletta, Glycosidic bond hydroxylation by polysaccharide monooxygenases, Trends Chem. 1 (2019) 198–209.

[28] D.L. Zechel, S.G. Withers, Glycosidase mechanisms: anatomy of a finely tuned catalyst, Acc. Chem. Res. 33 (2000) 11–18.

[29] S. Striegler, Q.H. Fan, N.P. Rath, Binuclear copper(II) complexes discriminating epimeric glycosides and $\alpha$- and $\beta$-glycosidic bonds in aqueous solution, J. Catal. 338 (2016) 349–364.

[30] M.S. Little, S.J. Pellock, W.G. Walton, A. Tripathy, M.R. Redinbo, Structural basis for the regulation of β-glucuronidase expression by human gut Enterobacteriaceae, Proc. Natl. Acad. Sci. U. S. A. 115 (2018) E152–E161.

[31] A.P. Bhatt, S.J. Pellock, K.A. Biernat, W.G. Walton, B.D. Wallace, B.C. Creekmore, M.M. Letertre, J.R. Swann, I.D. Wilson, J.R. Roques, D.B. Darr, S.T. Bailey, S. A. Montgomery, J.M. Roach, M.A. Azcarate-Peril, R.B. Sartor, R.Z. Gharaibeh, S. J. Bultman, M.R. Redinbo, Targeted inhibition of gut bacterial β-glucuronidase activity enhances anticancer drug efficacy, Proc. Natl. Acad. Sci. U. S. A. 117 (2020) 7374–7381.

[32] H. Wei, L. Gao, K. Fan, J. Liu, J. He, X. Qu, S. Dong, E. Wang, X. Yan, Nanozymes: a clear definition with fuzzy edges, Nano Today 40 (2021), 101269.

[33] J. Wu, X. Wang, Q. Wang, Z. Lou, S. Li, Y. Zhu, L. Qin, H. Wei, Nanomaterials with enzyme-like characteristics (nanozymes): next-generation artificial enzymes (II), Chem. Soc. Rev. 48 (2019) 1004–1076.

[34] D. Jiang, D. Ni, Z.T. Rosenkrans, P. Huang, X. Yan, W. Cai, Nanozyme: new horizons for responsive biomedical applications, Chem. Soc. Rev. 48 (2019) 3683–3704.

[35] Y. Sohtome, T. Shimazu, Y. Shinkai, M. Sodeoka, Propargylic *Se*-adenosyl-L-selenomethionine: a chemical tool for methylome analysis, Acc. Chem. Res. 54 (2021) 3818–3827.

[36] B. Faubert, A. Tasdogan, S.J. Morrison, T.P. Mathews, R.J. DeBerardinis, Stable isotope tracing to assess tumor metabolism in vivo, Nat. Protoc. 16 (2021) 5123–5145.

[37] T.K. Dayie, L.T. Olenginski, K.M. Taiwo, Isotope labels combined with solution NMR spectroscopy make visible the invisible conformations of small-to-large RNAs, Chem. Rev. 122 (2022) 9357–9394.

[38] H. Tao, L. Lauterbach, G. Bian, R. Chen, A. Hou, T. Mori, S. Cheng, B. Hu, L. Lu, X. Mu, M. Li, N. Adachi, M. Kawasaki, T. Moriya, T. Senda, X. Wang, Z. Deng, I. Abe, J.S. Dickschat, T. Liu, Discovery of non-squalene triterpenes, Nature 606 (2022) 414–419.

[39] S. Scott, H. Zhao, A. Dey, T.B. Gunnoe, Nano-apples and orange-zymes, ACS Catal. 10 (2020) 14315–14317.